Investigation of Heat Exchanger Improvement via Ultrasonic Energy

Experimental Study

by

Roshan Sameer Annam

A Thesis Presented in Partial Fulfillment
of the Requirements for the Degree
Master of Science

Approved April 2019 by the
Graduate Supervisory Committee:

Patrick Phelan, Chair
Konrad Rykaczewski
Ryan Milcarek

ARIZONA STATE UNIVERSITY

May 2019

ABSTRACT

In these times of increasing industrialization, there arises a need for effective and energy efficient heat transfer/heat exchange devices. The focus nowadays is on identifying various methods and techniques which can aid the process of developing energy efficient devices. One of the most common heat transfer devices is a heat exchanger. Heat exchangers are an essential commodity to any industry and their efficiency can play an important role in making industries energy efficient and reduce the energy losses in the devices, in turn decreasing energy inputs to run the industry.

One of the ways in which we can improve the efficiency of heat exchangers is by applying ultrasonic energy to a heat exchanger. This research explores the possibility of introducing the external input of ultrasonic energy to increase the efficiency of heat exchanger. This increase in efficiency can be estimated by calculating the parameters important for characterization of a heat exchanger, which are effectiveness (ε) and overall heat transfer coefficient (U). These parameters are calculated for both the non-ultrasound and ultrasound conditions in the heat exchanger.

This a preliminary study of ultrasound and its effect on a conventional shell-and-coil heat exchanger. From the data obtained it can be inferred that the increase in effectiveness and overall heat transfer coefficient upon the application of ultrasound is ~1% and 6.22% respectively.

ACKNOWLEDGMENTS

This study was conducted under the supervision and mentorship of Prof. Patrick Phelan and with the help from Hooman Daghooghi Mobarakeh in helping me with all the required insights for the manufacturing of the experimental setup and setting up of the experiment. I am also thankful to the help extended by USPCASE exchange student Hafiz Muhammad Hassan during the experimental work and also in the analysis of the date. I am also very thankful to all my family members and my friends for their continuous support and help during the course of my Master's degree.

TABLE OF CONTENTS

LIST OF TABLES

LIST OF FIGURES

NOMENCLATURE

Density	ρ	Reynolds Number	Re
Dynamic Viscosity	μ	Prandtl Number	Pr
Kinematic Viscosity	v	Nusselt Number	Nu
Specific heat of water	C_p		
Conductivity of Water	k_w	Volume Flow Rate	$\dot{V}$
Conductivity of Copper Tube	k_c	Hot Inlet Temperature	T_{hi}
Length of Coil	L	Hot Outlet Temperature	T_{ho}
Number of turns of Coil	N	Cold Inlet Temperature	T_{ci}
Velocity	V	Cold Outlet Temperature	T_{co}
Pith of the Coil	p	Surface Temperature	T_s
Coil Thickness	x	Far Field temperature	T_∞
Coil Tube Inner Diameter	d_i	Gravitational Acceleration	g
Coil Tube Outer Diameter	d_o	Coefficient of volume expansion	β
Helix Diameter	D_H	Characteristic Length	L_c
Annulus/Shell Diameter	D	Thermal Diffusivity	α
Internal Heat Transfer coefficient	h_i	Heat transfer from vertical wall	$\dot{Q}_V$
External Heat Transfer coefficient	h_o	Heat transfer from bottom horizontal surface	$\dot{Q}_{H,B}$

Overall Heat Transfer Coefficient	U_{Th}	Heat transfer from upper horizontal surface	$\dot{Q}_{H,U}$
Experimental Heat Transfer coefficient	U_{Exp}		

CHAPTER 1

INTRODUCTION

1.1 Ultrasonics and their application

The field of ultrasonics is considered to be a branch of acoustics which generally deals with the generation, propagation and different possible applications of these inaudible acoustic waves. All the frequencies which are greater than 20kHz (which are considered audible to human ears) come under the field of ultrasonics. This branch of acoustics can be categorized into [1]:

1. Low intensity, high frequency applications
2. High intensity, low frequency applications

In case of low intensity ultrasonics, the power supplied to the piezoelectric/piezoceramic transducer is very low (on the order of milliwatts) and the frequencies are on the order of megahertz. The other category of high intensity and low frequency application is regarded as 'Power Ultrasonics'. Here the power applied to a transducer is in the range of 10's, 100's and 1000's of Watts as required by the application, whereas frequencies with the order of magnitude of kHz are observed. Most observed frequencies lie between 20kHz to 100kHz and may go as high as 500kHz.

The field of power ultrasonics is applicable in the areas of acoustic saturation, radiation pressure, and microstreaming and cavitation in liquids, because of the effects created by the non-linear phenomena that are a result of the high-intensity waves. Some of the other effects created by the aforementioned non-linear phenomena are heat, agitation, diffusion, interface stabilities, friction,

mechanical rupture, and chemical effects [1].

1.2 Effect of ultrasound in fluids and fluid flow

The effects of acoustic cavitation (Figure 2), free surface deformation, convection (Figure 1) and acoustic streaming (Figure 3) are observed when power ultrasound is propagated through a fluid medium [2].

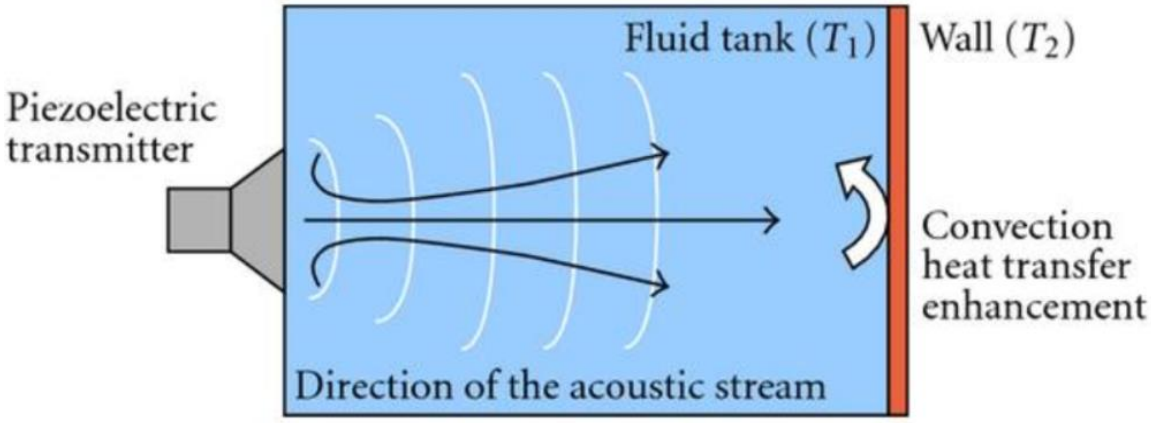

Figure 1: Convection in acoustic field

(*Source: Enhancement of Heat Transfer by Ultrasound: Review and Recent Advances, Mathieu Legay, Nicolas Gondrexon, Stephane Le Person,Primius Boldo and Andre Bontemps*)

Broadly speaking, cavitation (Figure 2) scan be loosely defined as the effects observed whenever there is a new film, or a new surface is created in a fluid medium. It can be observed in boiling and effervescence phenomena. Speaking specifically for acoustic cavitation, it is strictly confined to the cases where the effects of expansion and contraction simultaneously occur in a fluid medium [3].

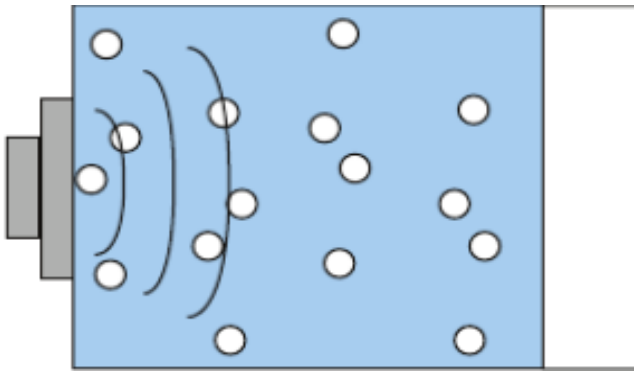

Figure 2: Acoustic cavitation

(Source: Enhancement of Heat Transfer by Ultrasound: Review and Recent Advances, Mathieu Legay, Nicolas Gondrexon, Stephane Le Person,Primius Boldo and Andre Bontemps)

Application of high intensity ultrasound may lead to cavitation in liquids which are important to many research applications. Cavities in a fluid medium can be described as an empty or a bounded volume containing gas or vapor. Superimposition of steady ambient pressure and time-varying (sinusoidal) pressure leads to generation of acoustic cavitation [4].

Gentle and violent responses can be observed in fluid when an acoustic field is applied. These can be referred to as stable and transient cavitation. Their response to the applied sound field depends on the pressure levels and other ambient conditions. These two types of cavitation are called transient (violent) and stable (gentle) respectively. Bubbles that non-linearly oscillate and continue oscillating for several cycles of time-varying pressure are called stable cavities. Whereas cavities which undergo rapid expansion and do not even last a single cycle of acoustic pressure are called transient cavities [4].

Now coming to the subject of acoustic streaming (Figure 3), the blanket definition of acoustic streaming is given as the streaming in a flowing fluid which is derived by time-averaged effects of its governing components [5].

Rayleigh [6][7] found the effects of acoustic streaming when he observed the motions of streaming which were caused by the introduction of standing waves between plane walls. Quartz winds is a streaming phenomenon discovered in modern times which is induced due to introduction of sound beams with high intensity produced by quartz oscillators [8]. Acoustic streaming can also be considered as the development of non-linear acoustic phenomena which are achieved by inducing a high intensity acoustic field in a steadily flowing fluid [9].

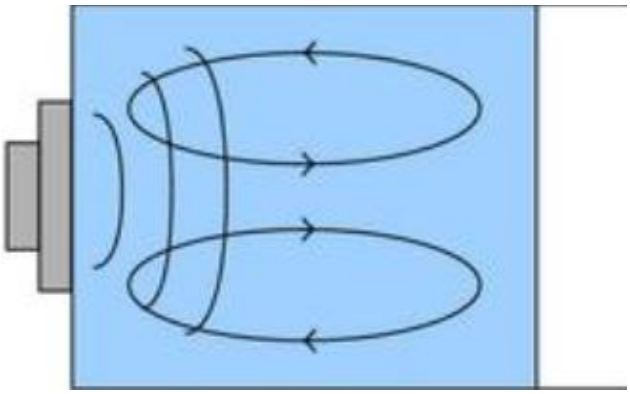

Figure 3: Acoustic streaming
(Source: Enhancement of Heat Transfer by Ultrasound: Review and Recent Advances, Mathieu Legay, Nicolas Gondrexon, Stephane Le Person,Primius Boldo and Andre Bontemps)

1.3 Effect of ultrasound in heat transfer

There are many references which have documented the effects of ultrasound on the process of heat transfer. Experiments conducted on preheated cylinders and spheres show that the acoustic streaming effect is responsible for an increase in the heat transfer [10]. An experimental study was conducted on the effects of high intensity ultrasound on the heat transfer to water flowing in an annular space. The rate by which the heat transfer increased was based on the amount of cavitation that occurred within the annular space and the flow regimes. An approximate increase of 40% was observed in the heat transfer coefficient of the process under non-boiling conditions [11].

Experiments conducted to identify the increase of heat transfer by boiling water and methanol were carried out. It was observed that there was an 8-fold increase in the heat transfer by convection, which was a result of increased cavitation of bubbles on the wire surface [12].

Liquid melting temperatures and melting times were observed for phase change materials (PCMs) under both ultrasound and non-ultrasound conditions. It was noted that there was a decrease in melting temperature and the melting time was 2.6 times faster for the PCM

in an ultrasonic field. The results also show that the increase in heat transfer caused due to the increased acoustic pressure [13].

Ultrasonic waves are thought to reduce liquid viscosity and assist the diffusion process, which in turn leads to increased heat transfer [14,15]. In the presence of an acoustic field, microstreaming phenomena occur at the solid layer, resulting in increased diffusion due to a reduction of the diffusion boundary layer, thus enhancing heat transfer capabilities [16]. Another contributing factor to enhanced heat transfer in pulsating acoustic fields is the creation of partial vacuum at liquid/solid interfaces [17].

Fluctuations in pressures induced by an acoustic field promote turbulence on the solid layer, enhancing heat transfer [18]. Other experiments included investigation of heat transfer in a miniaturized furnace. This experiment was carried out for a range of flow conditions. The acoustic field applied to the system was a low frequency (22-33 kHz) and high intensity (500-1000 W) acoustic/ultrasonic field. It was observed that sonification provided significant assistance in heat transfer in stagnant conditions [19].

Boiling heat transfer was improved by 17% using low power acoustic energy. This was achieved by increasing the critical heat flux by removing the bubbles accumulating at the heating surface, and also by reducing the factors which lead to the transition from nucleate to film boiling [20].

1.4 Effect of ultrasound on heat exchangers

Some experiments have been carried out on heat exchangers subject to an acoustic field. One of the first experiments in this particular area was carried out by Kurbanov and Melkumov. They reported an increase of 20% in the heat transfer process in a refrigeration system. They also noted that the use of ultrasound in the system reduced pumping friction,

in turn reducing pumping power, which was a result of the disruption of the boundary layer due to the presence of lubricating films [21].

Heat transfer in the presence of a low-frequency ultrasonic field has been investigated. In one of the experiments, ultrasonic energy was applied to a home-made shell-and-tube type heat exchanger, also known as a 'Sonoexchanger'. The overall heat transfer coefficient for both the non-ultrasound and ultrasound heat exchangers was determined. It was observed that under the effect of an acoustic field, an enhancement of 123% to 257% was observed in the overall heat transfer coefficient for the home-made ultrasonic heat exchanger. The comparison was made between the overall heat transfer coefficient (U) in both ultrasound and non-ultrasound conditions. This exchanger utilized a stainless-steel U-tube as the inner tube of the heat exchanger for the experiment. The above experiment used a 35-kHz ultrasonic transducer and the power of the transducer was calculated thermodynamically by measuring the increase in the temperature of the cold water in the system when the ultrasonic transducer was kept in the ON condition and there was no hot water flowing through the inner tube of the heat exchanger [22].

In another experiment done by the same group, a tube in tube heat exchanger and its working under the influence of ultrasonic energy was observed. The ultrasonically vibrating tube in the tube heat exchanger yielded a better overall heat transfer coefficient as compared to a simple tube-in-tube heat exchanger [23].

CHAPTER 2

APPROACH

The current experiment involves evaluation of the working parameters that are indicative of the efficiency of a shell-and-coil type heat exchanger. With the help of knowledge gained from the literature reviewed in this area, a heat exchanger was designed and fabricated with inlets and outlets provided for the flow of hot and cold water through the heat exchanger. An experimental setup with required instruments, equipment and assorted piping and valves was assembled for recording various temperature and flowrate measurements. The following section will describe the major factors that were taken into account during the design, fabrication and stages of assembly for the heat exchanger experimental setup.

2.1 Heat exchanger design and fabrication

Taking motivation from the literature review done in the field of the effect of ultrasound/acoustic field on the functioning of heat exchangers, the following steps were taken to develop the design and for the fabrication methodology for the heat exchanger.

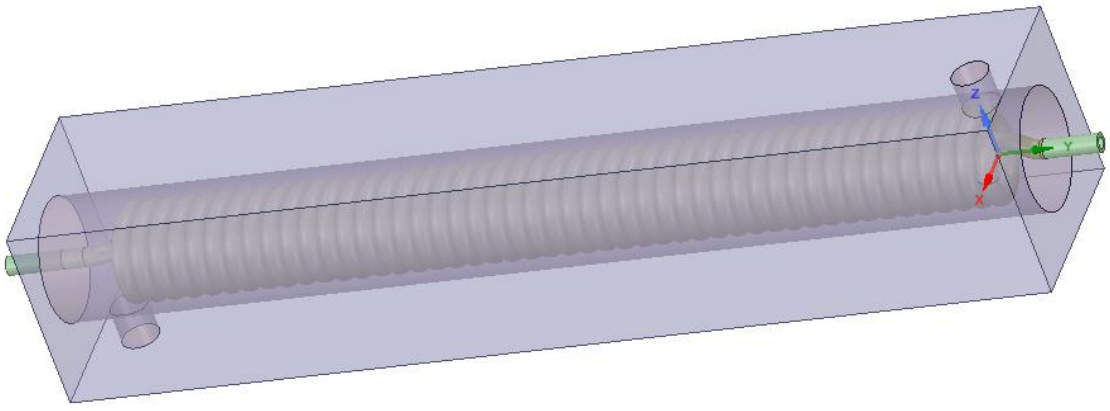

Figure 4: 3-D model of heat exchanger

Figure 4 is the 3-D model of the heat exchanger in question. The outer core is constructed by using an aluminum block with a square cross section.

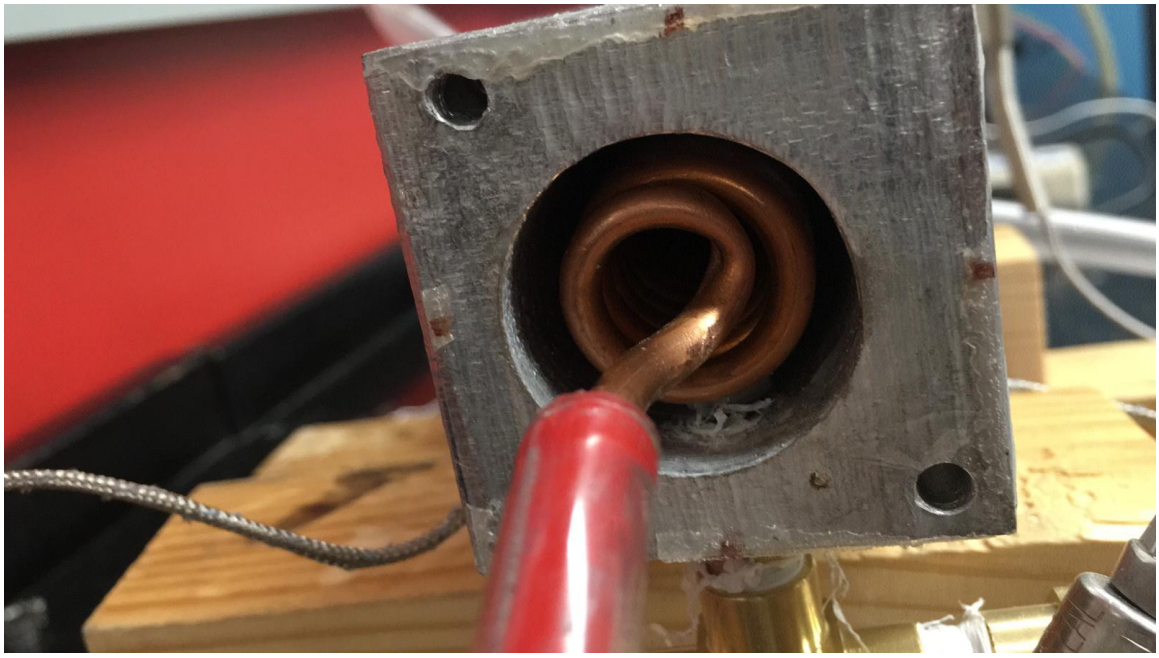

Figure 5: Cross section of heat exchanger

This outer core, as seen in Figure 5, is drilled and bored to create a cavity. This cavity encases the inner tube, which in this case is a coil made from copper tubing.

Figure 6: Copper coil as inner tube for exchanger

The copper tubing coil (Figure 6) is responsible for carrying hot water through it, which is the source of heat input to the system/heat exchanger. The reason behind selecting a copper coil as the inner tube was due to the excellent thermal properties of copper. The coil also provides a larger surface area through which heat transfer occurs which is significantly larger than the surface area available in a shell and U-tube type or a tube-in-tube type heat exchanger (in terms of the heat energy available for the system).

Another reason for the consideration of the copper coil as the inner tube for our experiment is its ease of manufacturability in the lab as compared to a U-tube which required bending machines of specific diameters of tube.

The tubing used has an inner diameter of 3 mm with a wall thickness of .75mm, which helps us to maintain turbulent flow regime for the hot fluid flowing through it. This is an advantage that we want to make use of in the system, ensuring that we can harness all the heat energy provided to the system.

The dimensions of the heat exchanger are described in Figure 7.

Figure 7: Dimensions of heat exchanger

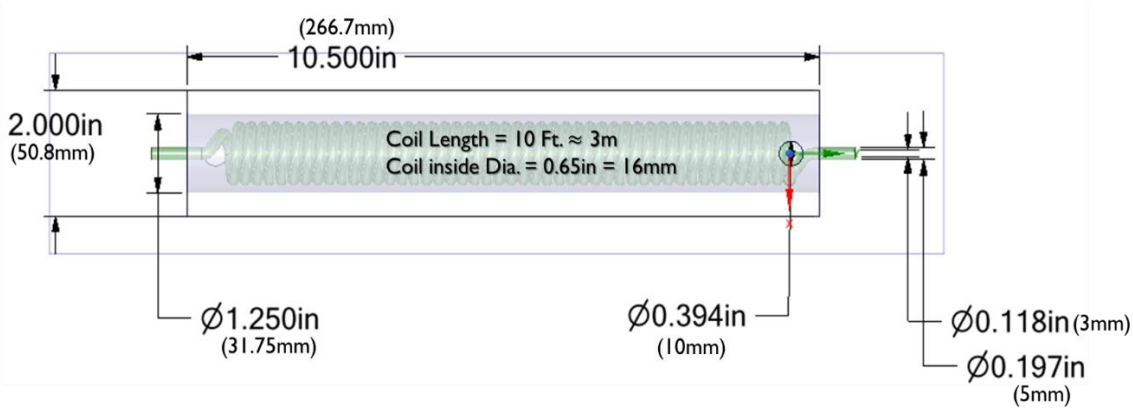

The cross-sectional area of the aluminum block used to fabricate the outer core of the heat exchanger is 5.08cm X 5.08cm (2in X 2in). The length of the heat exchanger is 10.5 inches

(close to the dimension of heat exchanger used in the reference papers [22] [23]). The inner diameter of the heat exchanger's aluminum core is 31.5mm (1.25 inches). The outer diameter of the coil is 4.83mm ($3/16^{th}$ inch) with a wall thickness of 0.76mm (0.03in). The total length of the helical coil is approximately 304cm (120 inches).

These turns on the coil are made in such a way that we make sure that there is no space between each consecutive turn (Figure 6). All the turns of coil are stuck together. This is done to be consistent with the pitch as winding the coil by hand cannot guarantee a consistent pitch across the length of the coil. The coil was made by winding the copper coil tubing on a copper tube of an outer diameter of 16.5mm (.65in).

Two holes of 3.18mm (1/8 inch) diameter are drilled on opposite faces and opposite ends of the outer core to make manifolds for the inlet and outlet for the shell side, which in this case has cold water running through it (Figure 8).

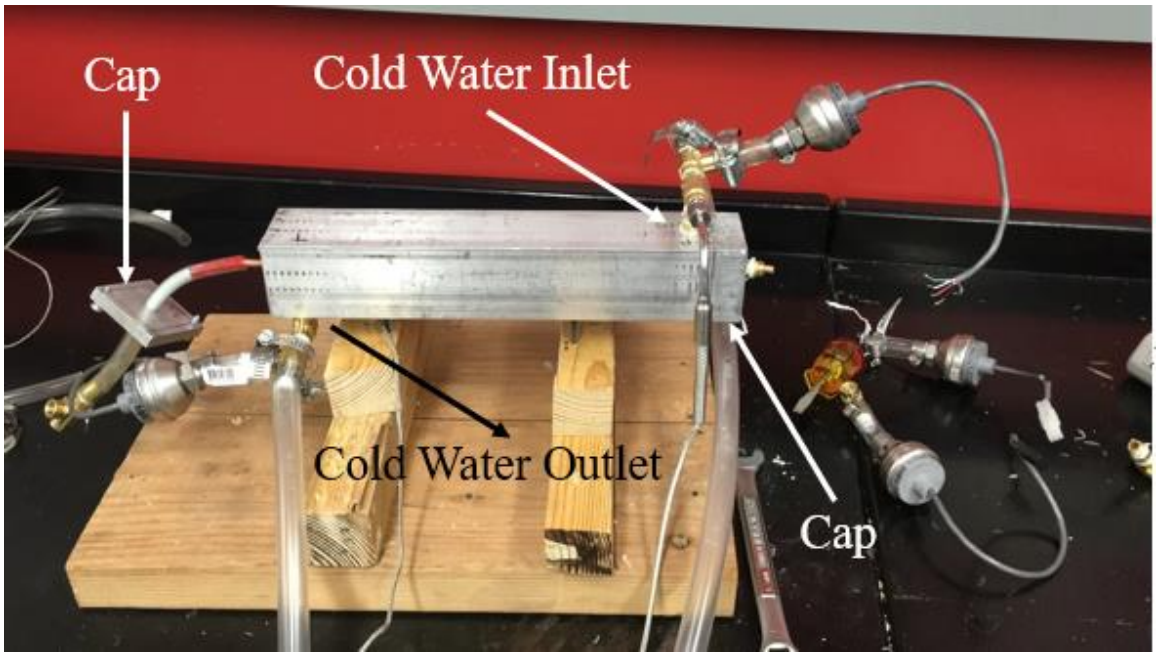

Figure 8: Caps for sealing and shell side inlet and outlet manifolds

Now to close the heat exchanger, 2 separate caps (square aluminum pieces) are cut out from the excess material (Figure 5). In these caps, holes are drilled and brass nipples of diameter 3mm are inserted through the holes in the cap and sealed with JB weld clear weld strong setting epoxy manufactured by JB weld company. This was done for both the caps. Next, the coil was placed inside the cavity of the aluminum block and caps were placed on the ends of the heat exchanger. The gap between the inner diameter of the brass nipple and the outer diameter of the copper tubing was filled with epoxy and the cavity was closed. The extensive use of epoxy was to avoid any kind of leakage, thus preventing any mixing of hot and cold water in the system. After this, the gaps created by the caps were filled with silicone sealant to ensure complete sealing and waterproofing.

A 40kHz 60W ultrasonic transducer (Figure 9) manufactured by Beijing Ultrasonics is attached to the outer core of the heat exchanger, along the length of the heat exchanger. The transducer is attached to the aluminum heat exchanger surface with the help of JB weld clear weld strong setting epoxy.

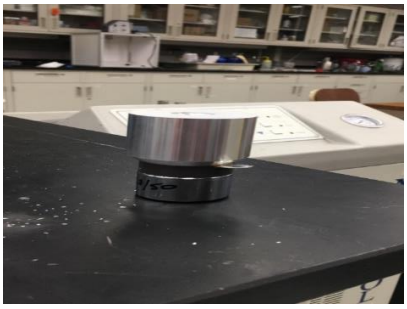

Figure 9: Ultrasonic transducer

The transducer is powered using a 40kHz PCB ultrasonic generator (Figure 10). The ultrasonic generator is manufactured by Beijing Ultrasonics.

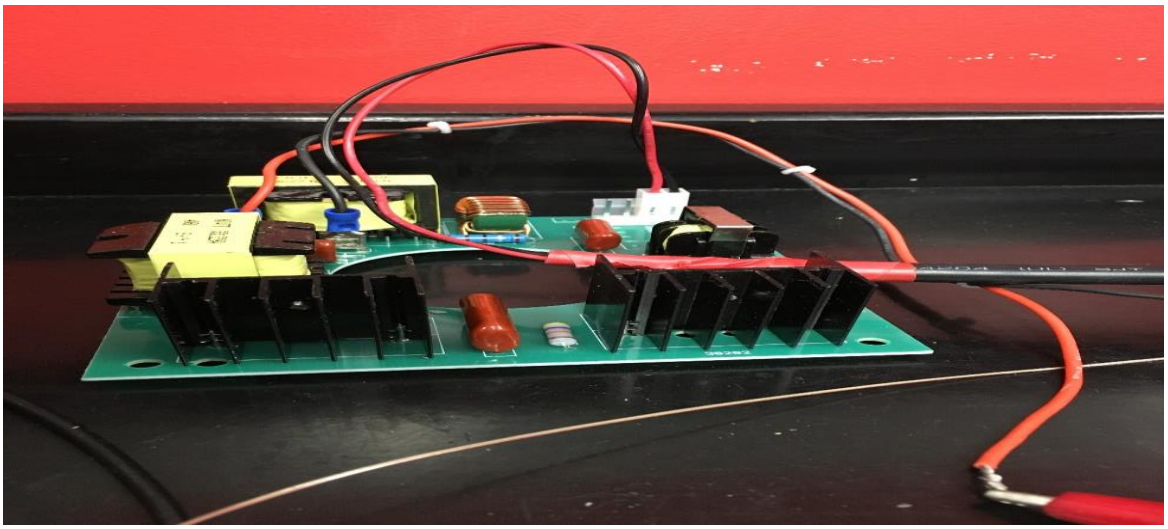

Figure 10: Ultrasonic generator

Insulation is applied to the heat exchanger to reduce any heat losses that might occur during the testing process. The insulation in question is a rubber insulation, with an adhesive back and has a thickness of 2mm. The insulation is manufactured by Ace Hardware.

Thermocouples for the experiment are fabricated in the lab, by using thermocouple wires, hot glue, super glue and 1/8th inch nipples. First, the thermocouple wires are stripped and wound together to make a tip which can measure temperature. After that these are sealed with super glue, so that water doesn't pass through the braids of the thermocouple and give us incorrect readings. Once the super glue dries, the thermocouple is then attached to the 1/8th inch nipple using hot glue sticks and hot glue gun, ensuring its rigidity and leak proofing.

2.2 Experimental setup

This experimental setup is designed to measure the 4 temperatures which are the hot inlet, hot outlet, cold inlet, and cold outlet. The heat exchanger surface temperature is also measured at three points during the experiment. Table 1 gives the detail of instrumentation used in the experimental setup.

Table 1: Instrumentation used in experimental setup

Instrument	Manufacturer	Model no.
Polystat® Thermal Bath	Cole-Parmer	BOM:2123338000
Eco 528 Submersible Pump	Ecoplus	S/N: 727715
Flowmeter (hot fluid)	King's Instrument Company (Liquid,0-1GPM)	S/N: 29400118004
Flowmeter (cold fluid)	King's Instrument Company (Liquid,0-4GPM)	K72-5/1 Series
Ultrasonic Transducer and Generator	Beijing Ultrasonics	_
Thermocouples (K-Type)	Omega Instruments	_
DAQ Board	Omega Instruments	(OM-DAQ-USB-2400 SERIES)

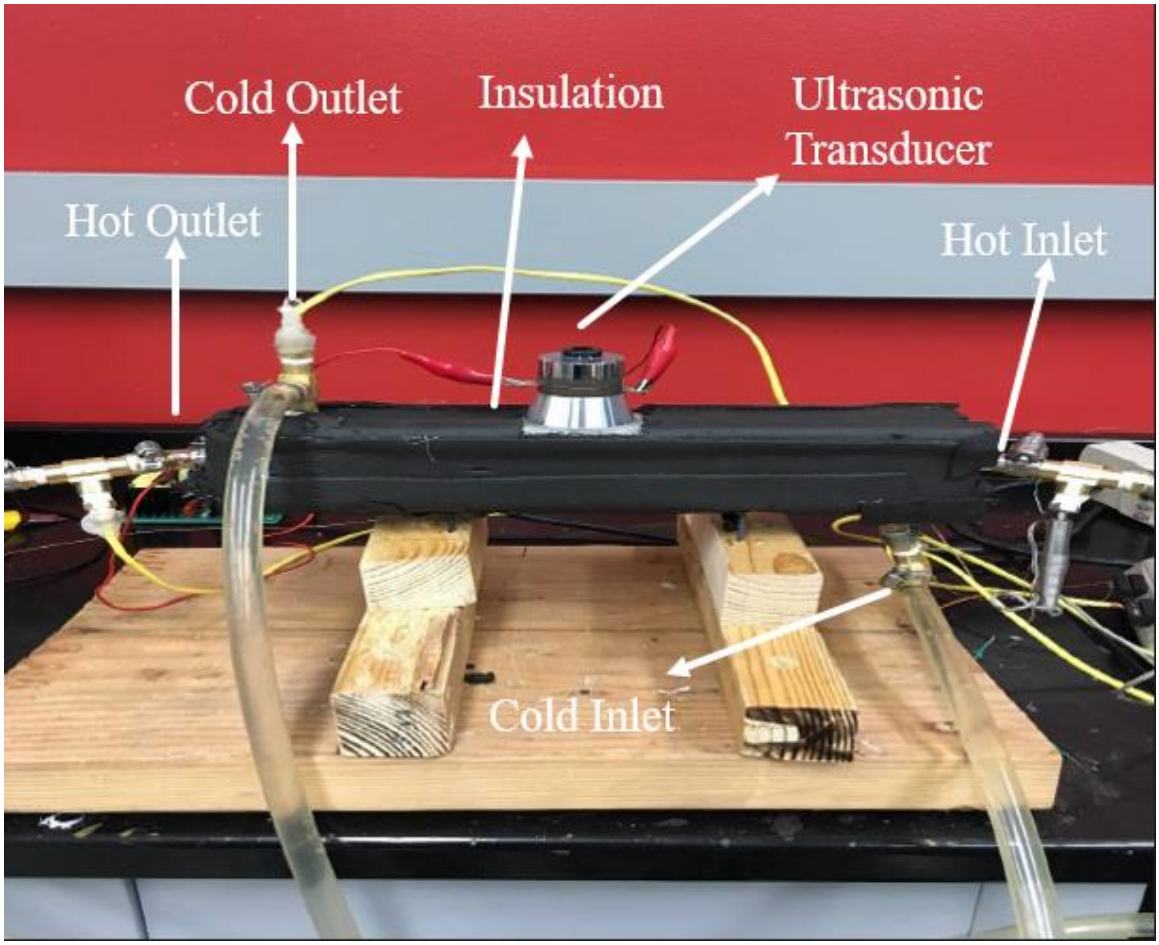

Figure 11: Experimental setup

Figure 11 gives us an idea about how the fabricated heat exchanger is prepared and assembled. The heat exchanger is placed on four metal nails drilled into the wooden structure which assists us ultrasonically by providing least resistance to flow of ultrasound by minimizing the contact surface area, reducing dissipation loss of acoustic field.

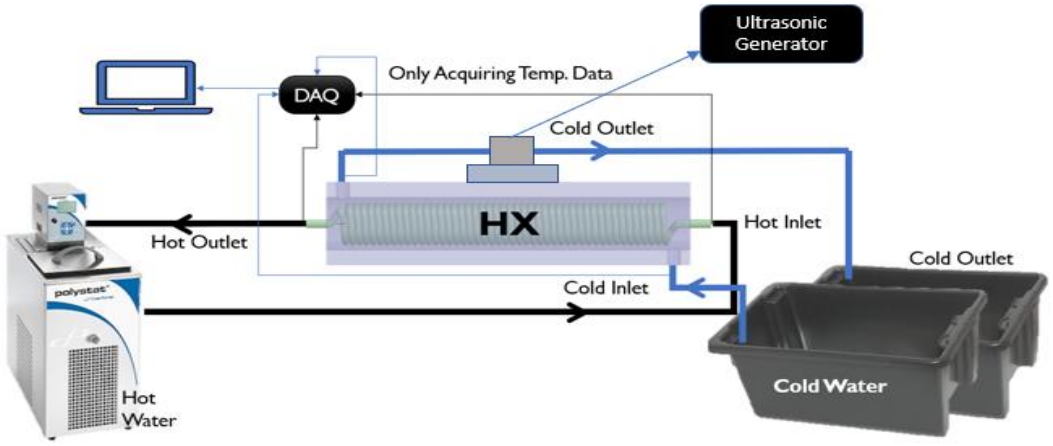

Figure 12: Schematic diagram

Figure 12 is a schematic diagram, indicating all the components used in the setup and also outlining the connections made to the components within the setup. The components required for the setup are:

- Polystat® Thermal bath
- Cold water reservoir
- Cold water return reservoir
- Ecoplus 528 submersible pump
- Ball valve
- Plastic pipes
- Brass T-connectors
- O-ring Clamps
- Thermocouples
- Ultrasonic Generator
- Data Acquisition Board

Figure 13: Thermal bath

From the setup schematic, it can be observed that the hot water is obtained with the help of a thermal bath (Figure 13). This is a Polystat® thermal bath manufactured by Cole-Palmer. It has a capacity of 15L. This thermal bath has a temperature range of -20 to 200 °C. It has an outlet and a return manifold which can be utilized for closing the hot water loop. The desired temperature is set on the thermal bath and the outlet and return are connected to each other like a bypass for the water in the bath to reach the desired temperature.

Once the temperatures are set, the pipe connecting the bath to the outlet and inlet of the hot water to the heat exchanger are connected to the return and supply manifold of the thermal bath respectively. This thermal bath has only two settings for flow of the water from the thermal bath. They are labelled as ‘LOW’ and ‘HIGH’ under the pump adjustment option. We can interchange between these two settings as desired.

Figure 14: Cold water reservoir and return

Next, tap water is used to fill the cold-water reservoir (Figure 14), which is the source of cold water for the experimental setup. The return of the cold water (cold outlet) is the sent

to a separate reservoir and not back into the cold reservoir. This is to avoid the change in the cold-water inlet conditions, thus keeping all the parameters constant.

Submersible pump (Eco Plus 528) is used to pump the cold water into the heat exchanger (Figure 15).

Figure 15: Submersible pump

This submersible pump has a maximum flow rate of 528 GPH. The volumetric flow rate of the pump can be altered by using the regulator at the front of the submersible pump. The pump was kept at max flow rate for our experiment. The same pump was then used to pump out the water from cold water return reservoir to make space in the reservoir for subsequent experiments.

A ball valve (Figure 16) is connected in between the cold-water inlet and the submersible pump, to provide the ease of changing the mass flow rate of cold water entering the system.

Figure 16: Ball valve

Four K-type thermocouples are used in the system (Figure 17) to measure the inlet and outlet temperatures of hot and cold water. Two K-type thermocouples are used to monitor the surface temperature in the experiment. These surface temperatures indicate the heat losses to be considered for the system during the energy balance.

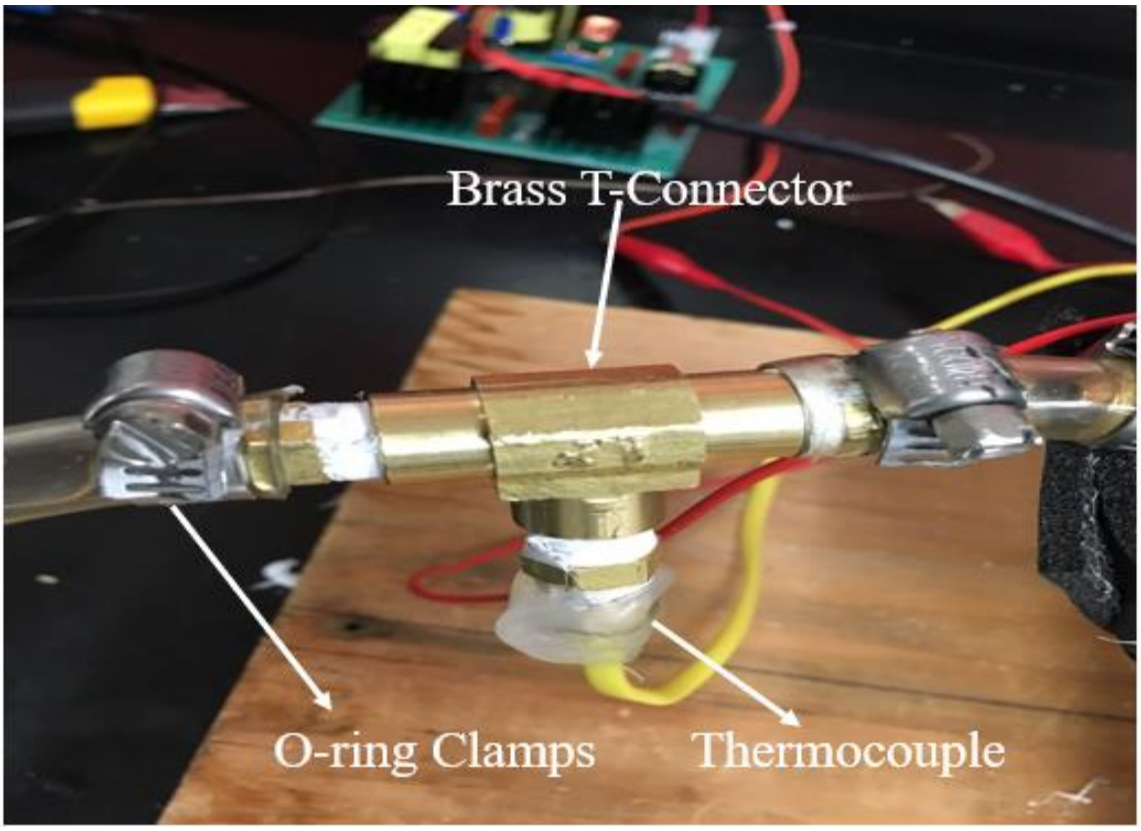

Figure 17: T connectors, O rings and thermocouple

These are custom made thermocouples, fabricated in the lab for the experiment. They are made using thermocouple wires and 1/8th inch nipples and hot glue. These thermocouples are connected to 1/8th inch female T joints which are locate at all the manifolds in the system. The setup is completed by using brass T-connectors and brass nipples with a diameter of 1/8th inch (3mm) to provide connections for inlet and outlet of hot and cold water as well as to connect the thermocouples to the system. The pipes and the connectors are secured by using the O-ring clamps, which prevent the possibility of any leakages in the system.

Once all the thermocouples are attached to the system, they are then connected to the Omega Data Acquisition Board (OM-DAQ-USB-2400 SERIES) in to the respective channels (Figure 18).

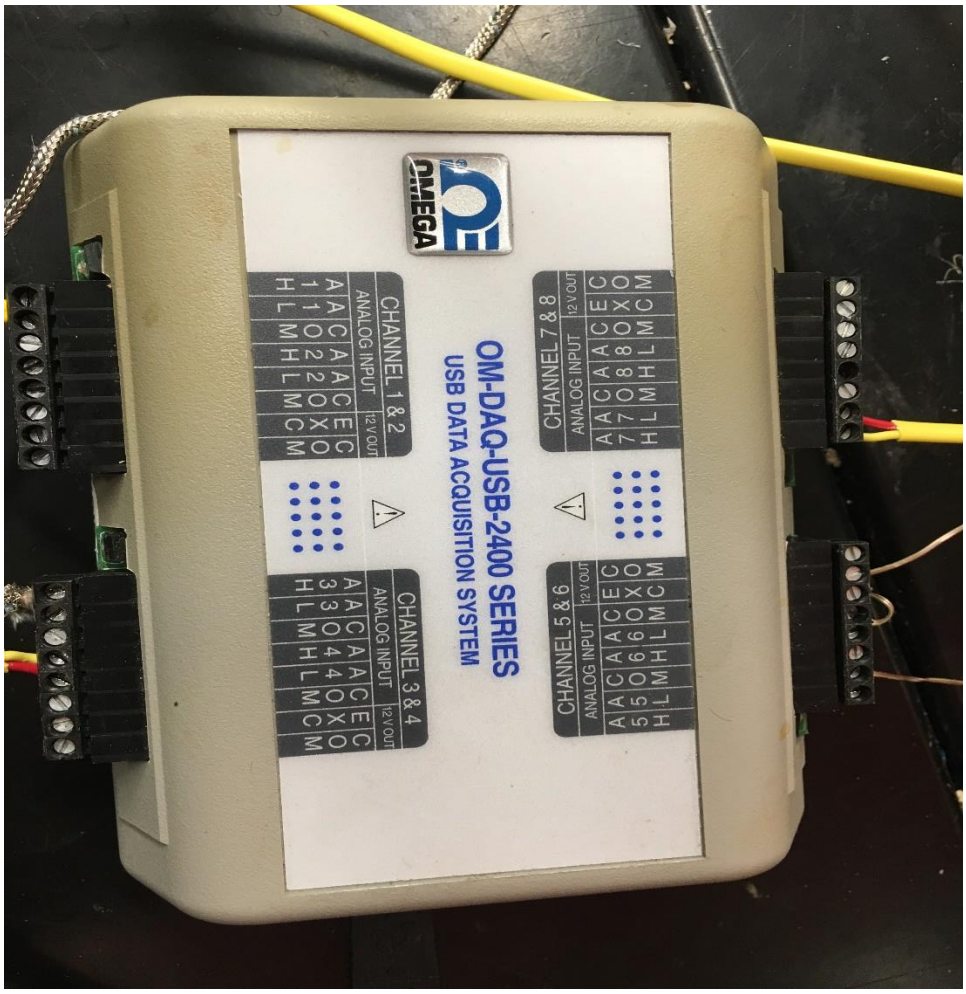

Figure 18: DAQ board

These channels are then configured into the software is utilized for recording the temperatures.

The sampling rate in this case is kept at 1 second as the system achieves a steady state in a while and there aren't many fluctuations in the temperature readings of the hot and cold-water inlets and outlets.

2.3 METHODOLOGY

In this section we are going to discuss the formulae that have been utilized for the analysis of the experiment conducted.

Energy balance for the whole system in general:

$$\dot{Q}_{hot} + P_{us} = \dot{Q}_{cold} + \dot{Q}_{env} \quad (1)$$

Now, we calculate the theoretical (non-ultrasound) and experimental (ultrasound) overall heat transfer coefficients (U) and effectiveness, to estimate the effect of ultrasound on the system.

To calculate the theoretical overall heat transfer coefficient, the following steps are required:

Convective heat transfer coefficient on the outer surface of the copper coil:
We first calculate the Reynold's number:

$$Re = \frac{\rho v d_i}{\mu} \quad (2)$$

Where d_i is the inner diameter of the copper coil. Then, we must choose the correlation for Nusselt Number based on the Reynolds number obtained. The flow is said to be laminar if $Re \leq 2{,}300$ and flow is said to be in turbulent regime, if $Re \geq 10{,}000$. Therefore [24]:

Circular tube, laminar ($Re \leq 2{,}300$)

$$Nu = {}^{h_i d_i}/_{k} = 3.66 \quad (3)$$

For Turbulent ($Re \geq 10{,}000$)

$$Nu = {}^{h_i d_i}/_{k} = 0.023 Re^{0.8} Pr^{n} \quad (4)$$

($n = 0.4$ heating & $n = 0.3$ Cooling)

Using the appropriate correlation, Nu is calculated, which gives us the value of h_i. Now for the case of a coil, this h_i is to be corrected as the above correlations are for a straight tube, which is done by the following formula [24].

h_i corrected for inside coil dia.

$$h_{ic} = h_i \left[1 + 3.5\left(\frac{d_i}{D_H}\right)\right] \tag{5}$$

h_i based on outside coil dia.

$$h_{io} = h_{ic}\left({}^{d_i}/_{d_o}\right) \tag{6}$$

Here h_{io} is the convective heat transfer coefficient of water inside the coil corrected for the outside diameter of the coil.

Following is the method for calculating the convective heat transfer coefficient for annular space between shell and coil:

Coil Length:

$$L = N\sqrt{(2\pi r)^2 + (p)^2} \tag{7}$$

Here, N is the number of turns on the coil and p is the pitch of the coil.

Volume occupied by the coil:

$$V_c = {}^{\pi}/_{4}\, d_o^2 L \tag{8}$$

Annulus Volume:

$$V_a = {}^{\pi}/_{4}\, D^2 l \tag{9}$$

Available volume for fluid flow:

$$V_f = V_a - V_c \tag{10}$$

Shell-side equivalent dia.:

$$D_e = {}^{4V_f}\Big/_{\pi d_o L} \tag{11}$$

For $50 \leq Re \leq 10{,}0000$:

$$Nu = {h_o D_e}/{k} = 0.6 Re^{0.5} Pr^{0.31} \quad (12)$$

For $Re \geq 10{,}000$:

$$Nu = {h_o D_e}/{k} = 0.36 Re^{0.55} Pr^{1/3} \left(\frac{\mu}{\mu_w}\right)^{0.14} \quad (13)$$

Once we have the values of the h_{io} and h_o, we can use the following relation to calculate the theoretical overall heat transfer coefficient.

Calculating the overall heat transfer coefficient (theoretical):

$$\frac{1}{U} = \frac{1}{h_o} + \frac{1}{h_{io}} + \frac{x}{k_c} \quad (14)$$

This $\frac{x}{k_c}$ term arises due to the conduction in coil. But since the thickness is very small, this term is generally neglected and hence then formula becomes:

$$\frac{1}{U} = \frac{1}{h_o} + \frac{1}{h_{io}} \quad (15)$$

Surface area of coil:

$$A_s = \pi d_o L \quad (16)$$

To calculate the overall heat transfer coefficient (experimental):

We first calculate the temperature difference in the system using log mean temperature difference (LMTD) method. There different correlations based on the orientation of the heat exchanger, whether it is a parallel or a counter flow heat exchanger. Since our experiment is on a parallel flow heat exchanger, the following equation is used:

Log Mean Temperature Difference (For Parallel Flow):

$$\Delta T_{LM} = \frac{(T_{hi} - T_{ci}) - (T_{ho} - T_{co})}{\ln {(T_{hi} - T_{ci})}/{(T_{ho} - T_{co})}} \quad (17)$$

Here, all the temperatures are the inlet and outlet temperatures of hot and cold water in the heat exchanger system. As seen above, we know the relation for the rate of heat transfer, and in this particular case, it can be modified as follows:

$$\dot{Q} = U_{exp} A_s \Delta T_{LMTD} \tag{18}$$

From the above equation, we are able to calculate the experimental overall heat transfer coefficient.

Effectiveness of the heat exchanger is given by the formula:

$$\varepsilon = \frac{\dot{Q}}{\dot{Q}_{max}} \tag{19}$$

Where $\dot{Q}_{max}$ is calculated by:

$$\dot{Q}_{max} = C_{min} \Delta T_{max} \tag{20}$$

Here C_{min} is the minimum of the following;

$$C_{min} = \min(C_c, C_h) \tag{21}$$

$$C_c = (\dot{m}_c C) \qquad C_h = (\dot{m}_h C) \tag{22}$$

$\dot{m}_c$ and $\dot{m}_h$ are the mass flow rates of hot and cold water, whereas C is the specific heat capacity of water.

To estimate the heat loss due to natural convection from the surface:

We first must calculate both Grashof and then Rayleigh numbers.

Grashof number:

$$Gr_L = \frac{g\beta(T_s - T_\infty){L_c}^3}{v^2} \tag{23}$$

Rayleigh number:

$$Ra_L = Gr_L Pr = \frac{g\beta(T_s - T_\infty){L_c}^3}{v\alpha} \tag{24}$$

Now using a table for the correlation of Nusselt Number for horizontal and vertical heating surfaces, we can calculate overall rate of heat transfer from the heat exchanger [25].

TABLE 9–1

Empirical correlations for the average Nusselt number for natural convection over surfaces

Geometry	Characteristic length L_c	Range of Ra	Nu	
Vertical plate 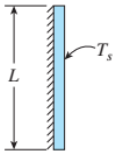	L	10^4–10^9 10^{10}–10^{13} Entire range	$Nu = 0.59Ra_L^{1/4}$ $Nu = 0.1Ra_L^{1/3}$ $Nu = \left\{0.825 + \frac{0.387Ra_L^{1/6}}{[1 + (0.492/Pr)^{9/16}]^{8/27}}\right\}^2$ (complex but more accurate)	(9–19) (9–20) (9–21)
Horizontal plate (Surface area A and perimeter p) (*a*) Upper surface of a hot plate (or lower surface of a cold plate)  (*b*) Lower surface of a hot plate (or upper surface of a cold plate) 	A_s/p	10^4–10^7 10^7–10^{11} 10^5–10^{11}	$Nu = 0.59Ra_L^{1/4}$ $Nu = 0.1Ra_L^{1/3}$ $Nu = 0.27Ra_L^{1/4}$	(9–22) (9–23) (9–24)

Figure 19: Nusselt number correlations as per the orientation of the plates

Using the above correlations, we can calculate the rate of heat loss for all the sides.

Therefore, the total heat loss from the heat exchanger becomes:

$$\dot{Q} = 2\dot{Q}_V + \dot{Q}_{H,B} + \dot{Q}_{H,U} \tag{25}$$

And to calculate the value of rate of heat loss for each individual surface:

$$\dot{Q} = hA_s(T_s - T_\infty) \tag{26}$$

2.4 Uncertainty analysis

The uncertainty of a calculated parameter *Y*, on the basis of the uncertainties in the primary measurements $x_1, x_2, x_3 \ldots$ [26]

$$Y = f(x_1, x_2, x_3 \ldots) \tag{27}$$

$$\Delta y = \sqrt{\left(\frac{\partial f}{\partial x_1}\right)^2 (\Delta x_1)^2 + \left(\frac{\partial f}{\partial x_2}\right)^2 (\Delta x_2)^2 + \left(\frac{\partial f}{\partial x_3}\right)^2 (\Delta x_3)^2 \ldots} \tag{28}$$

Now, the major parameters in our consideration are overall heat transfer coefficient (*U*) and effectiveness (ε).

Overall heat transfer coefficient:

$$U_{exp} = \frac{\dot{Q}}{A_s \Delta T_{LMTD}} \tag{29}$$

Effectiveness of the heat exchanger:

$$\varepsilon = \frac{\dot{Q}}{\dot{Q}_{max}} \tag{30}$$

The uncertainty calculations are done by using the general equation to calculate the uncertainty of measurement of each component and then the uncertainties of the overall heat transfer coefficient and effectiveness are calculated using a MATLAB code.

CHAPTER 3

RESULTS AND DISCUSSION

Before starting the experiment, it is necessary to find out the natural frequency of the ultrasonic transducer. The natural frequency of an ultrasonic transducer may vary, depending up on the system to which it is coupled. So, in a free (unloaded) and a coupled (loaded) condition, the natural frequency of the transducers is different. The transducer used for the experiment is 40kHz in unloaded condition. This is specified by the manufacturer. Once coupled to the heat exchanger, the natural frequency needs to be determined.

To do that, a oscilloscope, a function generator and an ultrasonic generator are required.

The frequencies are varied and the impedance to the transducer is calculated with the help of current and voltage values obtained from the oscilloscope. We also use a shunt resistor to determine the current reaching the transducer.

At natural frequency, the impedance to the transducer from the generator is the least and the transducer draws maximum power, which ensures maximum electrical power is converted into mechanical vibrations.

By following the steps mentioned above, we were able to determine the natural frequency of the transducer. It shifted to around 51.5kHz. Figure 20 gives us an idea about the natural frequency. The figure is a plot of Impedance vs Frequency and it is evident that the lowest possible impedance is observed at 51.5kHz.

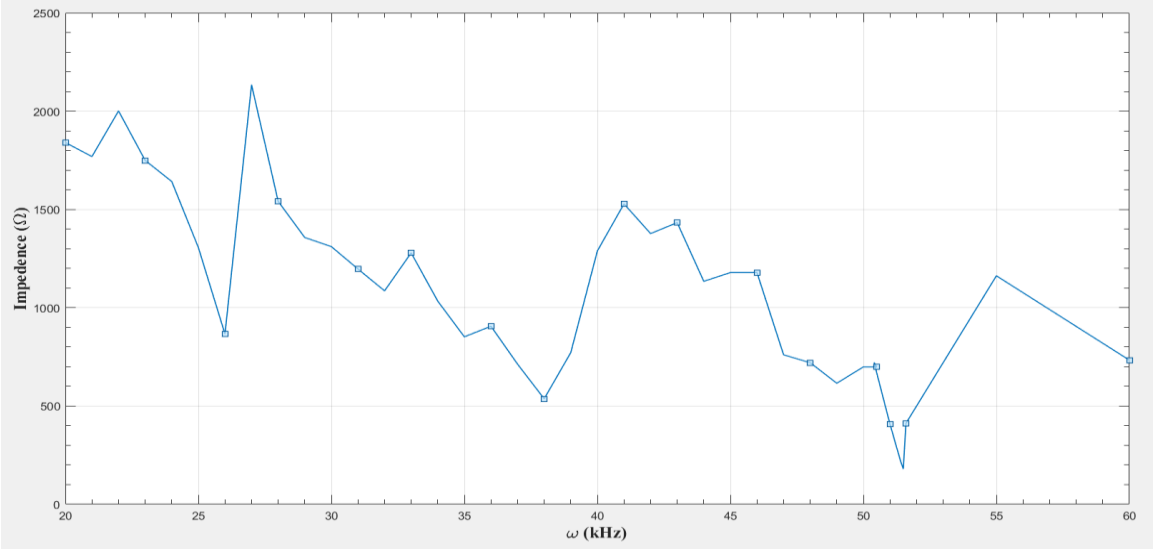

Figure 20: Estimation of natural frequency of loaded transducer

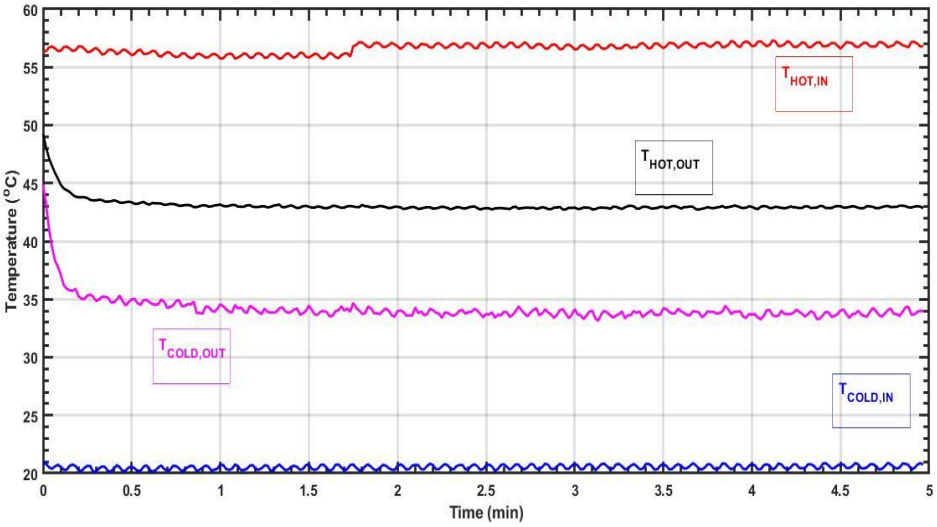

.

Figure 21: Temperature profiles of inlet and outlet of hot and cold water in non-ultrasound condition (Continuous Reading)

From Figure 21, it can be inferred that system reaches a steady state in and about 60-90 seconds. The figure represents the trend in the temperature of hot and cold water inlets and outlets when measured continuously in under the non-ultrasound condition. The graph also indicates the temperatures attained by the hot and cold water during the experiment. Also,

it can be observed that no fluctuations are observed in the readings caused by the ultrasonic transducer when it is on.

But, when the ultrasonic transducers are on, fluctuations were observed in the temperature measurements.

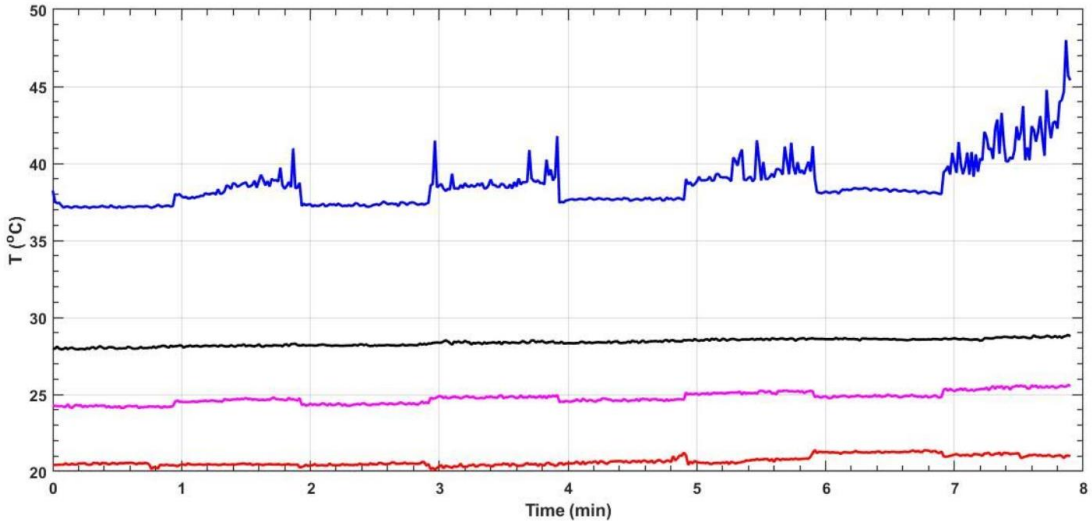

Figure 22: Inlet and outlet temperatures profiles of hot and cold water in both ultrasound and non-ultrasound

In figure 22, fluctuations are seen in some of the intervals and no fluctuations in other intervals. The intervals with fluctuations indicate temperatures recorded when ultrasound was on and vice versa. Therefore, the temperatures recorded while the transducer was on resulted in highly erroneous values.

To avoid the above fluctuations, a new way to record the temperatures was adopted. For temperature measurements when the transducer is on, the transducer is kept running for the first two minutes of the experiment. Now as we approach the 2-minute mark, the transducer is shut off and the data acquisition software is started. The software is run for 10 seconds and the software is switched of. Then again, the transducer is kept running for a minute. As it approaches the 3-minute mark, the transducer is again switched off and the

temperatures are recorded. This process is continued for the duration of experiment with ultrasound on.

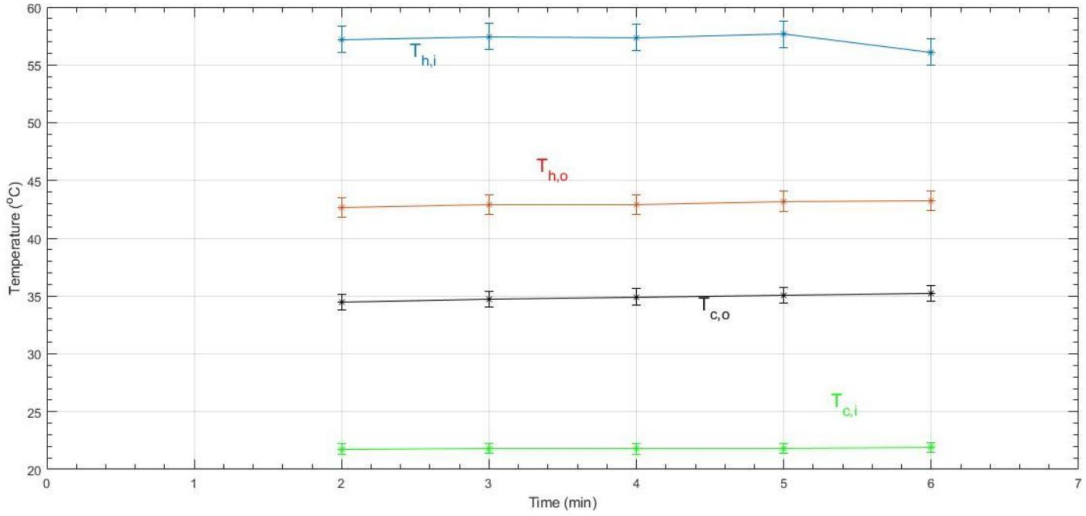

Figure 23: Plot of temperatures averaged at each minute under ultrasound conditions

Figure 23 shows the temperatures measured at the 2-minute mark and so on till 6 minutes. The temperatures plotted at the particular time stamp is the average of 10 temperature readings taken during the 10 seconds when the transducer was off.

A similar method was applied to the temperatures measured in the non-ultrasound condition as well so that we have a proper comparison of temperature profiles in both the ultrasound and non-ultrasound condition (Figure 24).

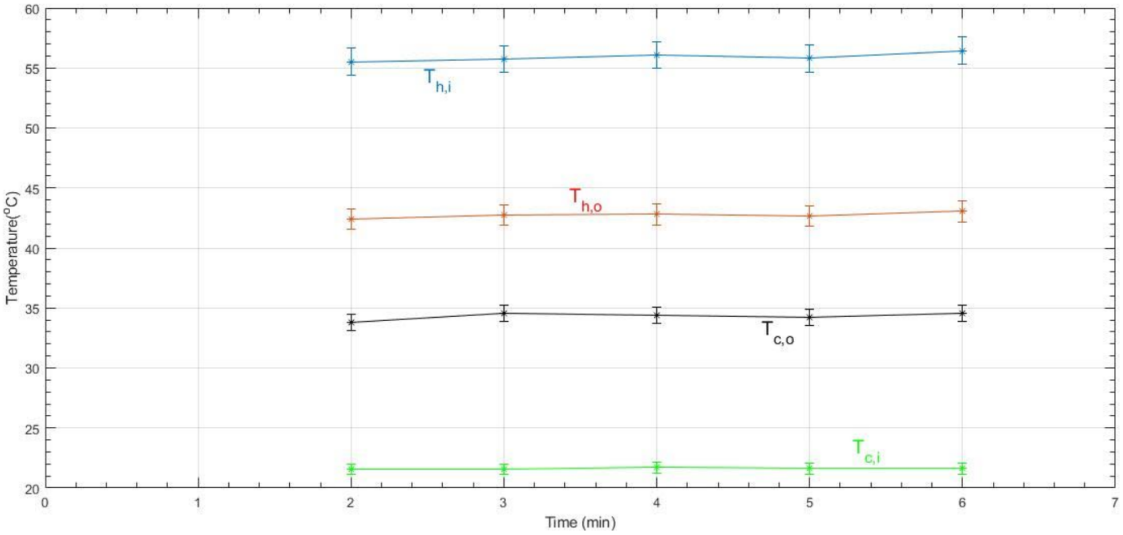

Figure 24: Plot of temperatures averaged at each minute under non-ultrasound conditions

Now, to calculate the heat losses due to natural convection, we assume that there is no insulation on the surface of the aluminum core. Tables 2 and 3 determine the boundary conditions and air properties for the calculations.

Table 2: Boundary conditions

Parameter	**Symbol**	**Value**	**Units**
Surface Temp	T_s	26.5	℃
Far Field Temp	T_∞	21	℃
Dimensions	$L \times H \times W$	10.5×2×2	in

Table 3: Air properties

Parameter	**Symbol**	**Value**	**Units**
Kinematic Viscosity	v	1.576E-05	m^2/s
Thermal Conductivity	k	0.0256	$W/_{mK}$
Thermal Diffusivity	α	2.161E-05	m^2/s
Co-efficient of Vol. Expansion	β	3.362E-03	K^{-1}
Prandtl Number	Pr	0.73	-

Table 4 gives us the values of Nusselt number and convective heat transfer coefficient at different surfaces of the heat exchanger outer core.

Table 4: Nusselt number and convective heat transfer coefficient values at different surfaces for heat loss calculation

Orientation	$\boldsymbol{Nu}$	$\boldsymbol{h}$
Vertical Surface	8.4746	4.2742
Bottom Surface	5.3819	2.0681

Top Surface	11.7604	4.5192

From the values in Table 4 and using equations (25) and (26) the heat loss due to natural convection without any insulation is 1.13 W. Hence, the heat loss is neglected from the energy balance equations.

Using equations (17) through (22), we calculate the overall heat transfer coefficient (Figure 25) and the effectiveness (Figure 26) of the heat exchanger in both the ultrasound and non-ultrasound conditions (experimentally).

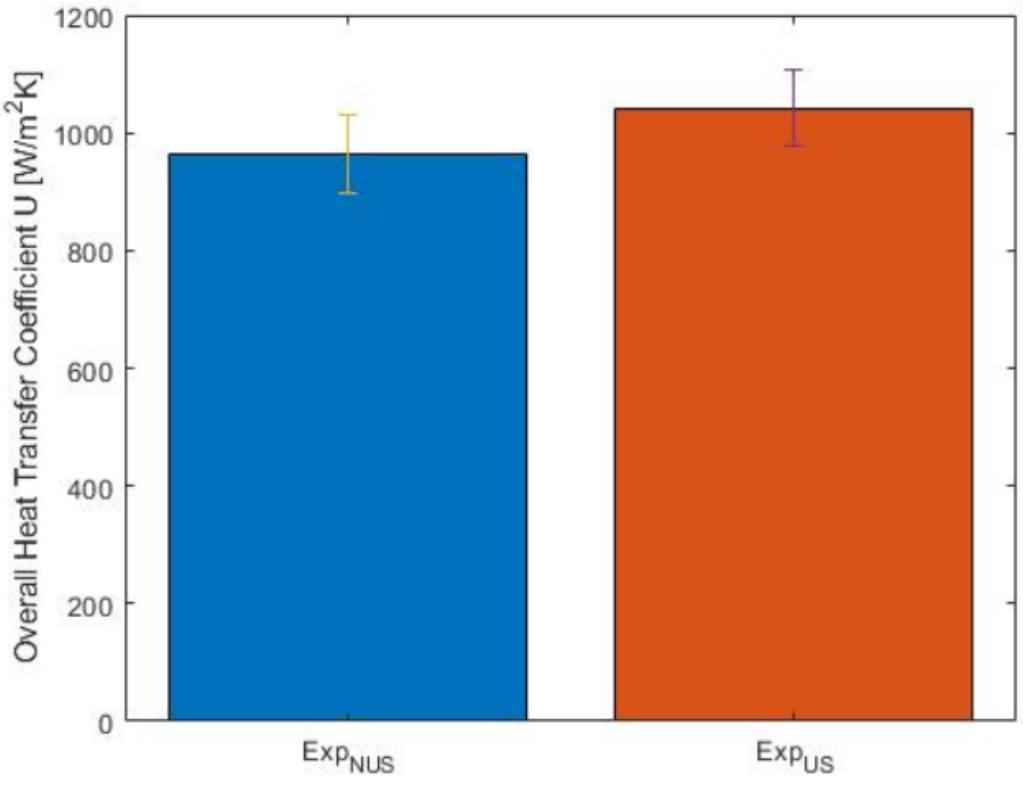

Figure 25: Comparison of overall heat transfer coefficients in non-ultrasound and ultrasound conditions

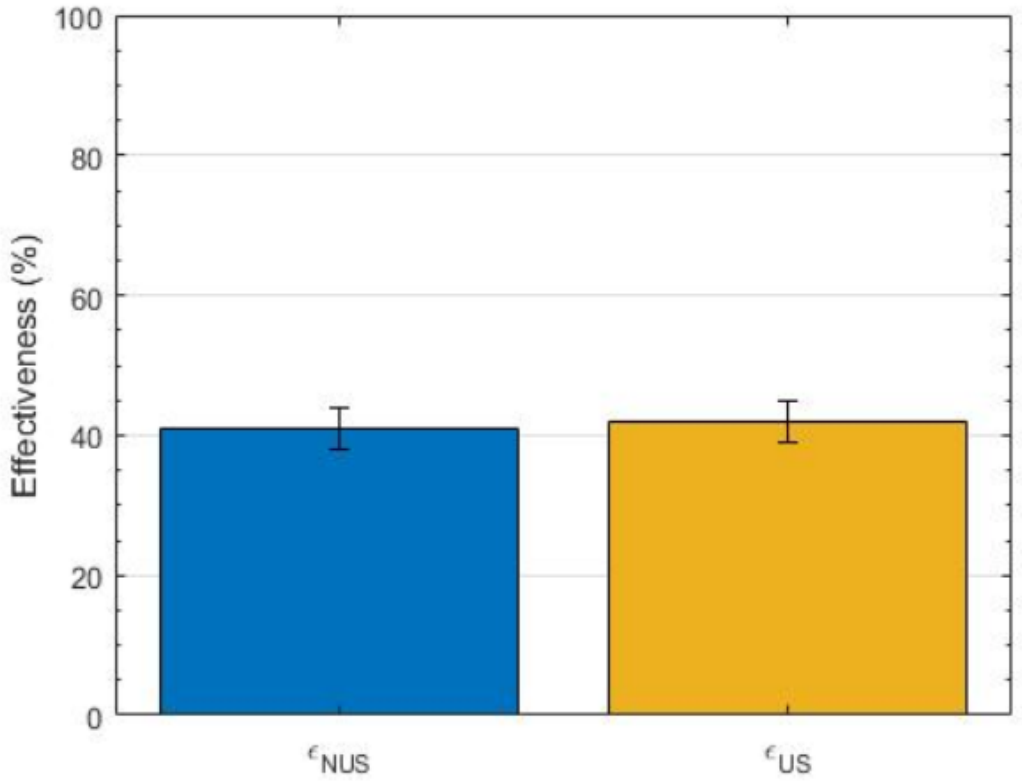

Figure 26: Comparison of effectiveness in non-ultrasound and ultrasound conditions

Table 5 gives us brief look into the comparison of parameters in both the ultrasound and non-ultrasound experiments.

Table 5: Parameter comparison between ultrasound and non-ultrasound experiments

Parameter	Non-Ultrasound	Ultrasound
$T_{cold,in}$ (°C)	20.58	21.81
$T_{cold,out}$ (°C)	33.79	34.89
$T_{hot,in}$ (°C)	56.88	57.15
$T_{hot,out}$ (°C)	42.89	42.98
ΔT_{cold} (°C)	13.21	13.10

ΔT_{hot} (°C)	13.98	14.17
$\dot{Q}$ (W)	921.93	912.69
$\dot{Q}$max (W)	2247.30	2187.77
ε	41%	42%
U (W/m^{2}K)	964	1024

From the above results, it can be observed that the addition of the ultrasound to the heat exchanger seems to increase its effectiveness and its overall heat transfer coefficient. The increment of 1% and 6.2% lies in the zone of uncertainty levels of the devices which are used to measure the parameters.

The uncertainty of effectiveness and overall heat transfer coefficient is ±7% respectively. This minute increment can be attributed to the fact that the power that the transducer draws from the power source is 5W and it is not clear whether the system receives all 5W because ultrasonic waves can get reflected, converted into heat, dissipated in air and may not propagate properly in the presence of discontinuous media. Acoustic wave dispersion is also a possibility.

The system draws only 5W of supplied power instead of 60W given by the generator. This is due to the frequency mismatch between the generator and the natural frequency of the ultrasonic transducer coupled to the system.

CHAPTER 4

CONCLUSION

From the experiments conducted, an increment of 6.2% and 1% in the overall heat transfer coefficient and effectiveness of heat exchanger is observed respectively. This increment lies in the uncertainty regions of the devices used for measuring the parameters in the experiment.

The generator board has a fixed frequency of 40kHz whereas the natural frequency of the transducer coupled to the heat exchanger is 51.5kHz. Due to the above mismatch, the power drawn by the transducer is only 5W which is **200** times less that the rate of heat transfer occurring in the heat exchanger.

Out of the 5W of energy drawn, only a certain percentage of that energy goes through as mechanical waves, considering the efficiency of the transducer in converting electrical energy into vibrational energy. Some of the generated wave is reflected, is dissipated at the interface (outer aluminum core), or gets converted into heat, which are not of help to us.

Using a generator with the operating frequency closer to the new natural frequency is advisable. Reducing the temperature of hot water to be supplied to the system can also be done so that the difference between the ultrasonic power in comparison to the heat transfer in the system is reasonably in proportion.

CHAPTER 5

FUTURE SCOPE

This study was a comparative study to identify whether the idea of the ultrasonic heat exchanger works or not. As discussed above, it does work. But to make our argument concrete, we need to make changes to the experiment. One way the results can be improved is by using an ultrasonic generator whose frequency is closer to the new shifted natural frequency. A generator with more power can be used so that the transducer can take in more energy.

This area of heat transfer has not been highly researched, hence there are a lot of open-ended things which can be sought. It will be interesting to see whether the orientation of the transducer plays any role in change in effective of ultrasonic heat exchanger. Its effect in various flow regimes of transient and turbulent flow can also present a greater picture.

Monitoring the pressure drop during the process is also important as it can be a deciding factor on whether the ultrasound increases or decreases the pressure drop, resulting in increased or decreased pump work, leading to less energy inputs and efficient devices.

REFERENCES

[1] Juan A. Gallego-Juarez and Karl. Graff. Power Ultrasonics: Applications of High-Intensity Ultrasound. Woodhead Publishing, Sawston, Cambridge, UK, 2014.

[2] J-L Laborde, A Hita, J-P Caltagirone: Fluid dynamics phenomena induced by power ultrasounds, 'Ultrasonics', Vol-38, March 2000, Pages: 297-300

[3] E A Neppiras, Acoustic Cavitation: Physics Reports, Vol-61 Issue 3, May 1980, Pages: 159-251

[4] E A Neppiras, Acoustic Cavitation Series: Part One: Acoustic Cavitation: An Introduction, Ultrasonics, Vol-22 Issue 1, May 1984, Pages: 25-28

[5] N Riley, Theoretical Computational Fluid Dynamics: Vol-10, 1998, Pages: 349-356

[6] Rayleigh, Lord (1883), Philos. Trans. Roy. Soc. London Ser. A, Vol. 175, pp. 1–21.

[7] Rayleigh, Lord (1896), The Theory of Sound, MacMillan, London.

[8] Meissner, A. (1926), Z. Tech. Physik, Vol. 7, pp. 585–595.

[9] C E Bradley, The Journal of Acoustical Society of America, Vol-100 Issue 3, 1996, 1399

[10] Yu.A. Borisov, Yu.G. Statnikov, Fizicheskii Zhurnal, Vol-13 Issue 3, 1967. Pages: 353

[11] A.E. Bergles, P.H. Newell The Influence of Ultrasonic Vibrations on Heat Transfer to Water Flowing in Annuli, International Journal for Heat and Mass Transfer, Vol-8, 1965, Pages 1273-1280

[12] M.B. Larson, A study of the effects of ultrasonic vibrations on convective heat transfer in liquids, Ph.D. Dissertation, Stanford University, Mic, 1961, pp. 61–1235.

[13] Y.K. Oh, S.H. Park, Y.I. Cho, A study of the effect of ultrasonic vibrations on phase-change heat transfer, Int. J. Heat Mass Trans. 45 (2002) 4631–4641.

[14] Gallego-Juárez, J.A., Rodriguez-Corral, G., Gálvez Moraleda, J.C., Yang, T.S., "A new high-intensity ultrasonic technology for food dehydration," Drying Technology, 17(3), pp. 597-608, (1999).

[15] Borisov, Y.Y. and Gynkina, N.M., "On acoustic drying in a standing sound wave," Soviet Physics-Acoustics, 8(1), pp. 95-96, (1962).

[16] Soloff, R.S., “Sonic drying,” Journal of the Acoustical Society of America, 36(5), pp. 961-965, (1964).

[17] Muralidhara, H.S., Chauhan, S.P., Senapati, N., Beard, R., Jirjis, B., Kim, B.C., “Electro-Acoustic Dewatering (EAD) a Novel Approach for Food Processing, and Recovery,” Separation Science and Technology, 23(12-13), pp. 2143-2158, (1988).

[18] Moy, J.H. and DiMARCO, G.R., “Exploring airborne sound in a nonvacuum freeze-drying process,” Journal of Food Science, 35(6), pp. 811-817, (1970).

[19] N.P. Dhanalakshmi, R. Nagarajan, N. Sivagaminathan, B.V.S.S.S. Prasad, Acoustic Enhancement of Heat Transfer in Furnace Tubes, Chemical Engineering, Vol-59, 2012, Pages: 36-42

[20] Zachary Douglas, Thomas R. Boziuk, Marc K. Smith, and Ari Glezer, PHYSICS OF FLUIDS 24, 052105 (2012)

[21] U. Kurbanov, K. Melkumov, Use of Ultrasound for Intensification of Heat Transfer Process in Heat Exchangers, 4, Proc. Int. Cong. Refr., Washington, D.C, 2003, 1-5.

[22] N. Gondrexon, Y. Rousselet, M. Legay, P. Boldo, S. Le Person, A. Bontemps, Intensification of heat transfer process: Improvement of shell-and-tube heat exchanger performances by means of ultrasound, Chemical Engineering and Processing, Vol-49, 2010, Pages 936-942

[23] N. Gondrexon, Y. Rousselet, M. Legay, P. Boldo, S. Le Person, A. Bontemps, Improvement of heat transfer by ultrasound: Application to a double-tube heat exchanger, Ultrasonic Sonochemistry, Vol-19, 2012, Pages 1194-1200

[24] Ramchandra K Patil, B.W. Shende, Prashanta K Ghosh, Designing a helical coil heat exchanger

[25] Heat and Mass Transfer, Fundamentals and Applications, Yunus A. Cengel, Afshin J. Ghajar

[26]http://www.sjsu.edu/people/ananda.mysore/courses/c1/s0/ME12011_Uncertainty_Analysis.pdf

APPENDIX

A: MATLAB CODE

```
%% Air Properties
beta_a=3.362e-3;
nu_a=1.576e-5;
alpha=2.1611e-5;
Pr_a=.73;
k_a=.025621;
%% Values
T_s=26.5;
T_infinity=21;
g=9.81;
%% Vertical Wall
L_v=0.0508;
Ra_v=(g*beta_a*(T_s-T_infinity)*L_v^3)/(nu_a*alpha);
Nu_v=(.825+(.387*Ra_v^(1/6))/(1+(.492/Pr_a)^(9/16))^(8/27))^2;
h_v=Nu_v*k_a/L_v;
%% Horizontal Wall
l=10.5*.0254;
w=2*.0254;
p=(4*w);
A1=l*w;
L_h=A1/p;
Ra_h=(g*beta_a*(T_s-T_infinity)*L_h^3)/(nu_a*alpha);
if (Ra_h>=10^4)&&(Ra_h<=10^7)
    Nu_hu=.59*Ra_h^(1/4);
elseif (Ra_h>=10^7)&&(Ra_h<=10^11)
    Nu_hu=.1*Ra_h^(1/3);
end
h_u=Nu_hu*k_a/L_h;
if (Ra_h>=10^4)&&(Ra_h<=10^11)
    Nu_hl=.27*Ra_h^(1/4);
end
h_l=Nu_hl*k_a/L_h;

Q=((h_v*2*A1)+(h_u*A1)+(h_l*A1))*(T_s-T_infinity);

%% Required Data
% All Units are in SI
x=xlsread('NUS.xlsx','Sheet1','A3:E7');

Q_c=.8*1.6667e-5;           % Mass Flow Rate (Cold Water)
T_c_i=x(:,4);       % Cold Water Inlet Temperature
T_h_i=x(:,2);       % Hot Water Inlet Temperature
T_c_o=x(:,5);       % Cold Water Outlet Temperature
```

```
T_h_o=x(:,3);       % Hot Water Outlet Temperature
%% Dimensions of Exchanger
l=10.5*.0254;      % Aluminum Block Length
D_i_i=.003;        % Inner Tube Inner Dia
D_i_o=.005;        % Inner Tube Outer Dia
D_o_i=1.25*.0254;          % Outer Tube Inner Dia
D_c=.021;            % Coil Dia
N=46;              % Number of Turns
p=.005;              % Pitch
%% Cold Water Properties
C_p_c=4179.2;        % Specific Heat
rho_c=996.6;         % Density
k_w_c=.6102;         % Themal Conductivity
mu_c=.0008538;       % Dynamic Viscosity
Pr_c=5.852;
%% Hot Water Properties
C_p_h=4179.7;        % Specific Heat
rho_h=990.7;         % Density
k_w_h=.6352;         % Themal Conductivity
mu_h=.0006131;       % Dynamic Viscosity
Pr_h=4.033;
%% Aluminum Properties
k_al=237;            % Themal Conductivity

%% Copper Properties
k_c=401;             % Themal Conductivity


%% Opening Commands
fopen('Helix_Inputs.m'); % To take inputs from Inputs.m file
run('Helix_Inputs');
%% Calculations
% h_i
%m_h=0.0148;
m_h=rho_c*Q_c*C_p_c.*(T_c_o-T_c_i)./(C_p_h.*(T_h_i-T_h_o));
Q_h=m_h./rho_h;
A_c_i=pi.*(D_i_i).^2/4;
v_i=Q_h./(A_c_i);
Re_h=rho_h.*v_i.*D_i_i./mu_h;
if Re_h<=2300
    Nu_h=4.36;
else
    Nu_h=0.023.*Re_h.^0.8.*Pr_h^(1/3);
end
h_i=Nu_h.*k_w_h./D_i_i;
h_ic=h_i*(1+3.5*(D_i_i/D_c));
h_io=h_ic*(D_i_i/D_i_o);
% h_o
L=N*sqrt((pi*D_c)^2+p^2); % Total Length of Inner Tube
V_c=pi*D_i_o^2*L/4;       % Volume of Coil
V_f=pi*D_o_i^2*l/4-V_c;   % Volume for Fluid Flow
D_e=4*V_f/(pi*D_i_o*L);   % Effective/Hydraulic Dia
G=(Q_c*rho_c)/((pi/4)*(D_o_i^2-((D_c+D_i_o/2)^2-(D_c-D_i_o/2)^2)));
Re_c=G*D_e/mu_c;
if (50<=Re_c)&&(Re_c<=10000)
    h_o=0.6*Re_c^0.5*Pr_c^.31*k_w_c/D_e;
else
```

```
    h_o=.36*Re_c^.55*Pr_c^(1/3)*k_w_c/D_e;
end
U=1./(1./h_o+1./h_io+((D_i_o-D_i_i)/2)./k_c);
U_mean=mean(U);
DeltaT_LM=((T_h_i-T_c_i)-(T_h_o-T_c_o))./log((T_h_i-T_c_i)./(T_h_o-
T_c_o));
DeltaT_LM=.99.*DeltaT_LM;        % Correction for Perpendicular Flow
A_s=pi.*D_i_o.*L;
Q=U.*A_s.*DeltaT_LM;

Cc=rho_c*Q_c*C_p_c;
Ch=rho_h*Q_h*C_p_h;
C_min=min(Cc,Ch);
Q_max=C_min.*(T_h_i-T_c_i);
ep=Q./Q_max.*100;
ep_1=mean(ep);

time=x(:,1);
thi=x(:,2);
tho=x(:,3);
tci=x(:,4);
tco=x(:,5);

Del_T_Hot=thi-tho;
Del_T_Cold=tco-tci;
Q1=.8*1.6667e-5*996.6*4179.2.*Del_T_Cold;
Q_exp=mean(Q1);
ep_exp=Q_exp./Q_max.*100;
ep_exp=mean(ep_exp);
figure (1)
plot(time,Q1,'*r-',time,Q,'*k-')
xlabel('Time [min]')
ylabel('Q [w]')
legend('Experimental','Theoretical')
%  axis([0 7 200 300])
set(gca,'XMinorTick','on','YMinorTick','on')
title(' ');
DelQ=Q1-Q;
Q2=mean(DelQ);
figure (2)
plot(time,DelQ,'*b-',3.5,Q2,'*k')
xlabel('Time [min]')
ylabel('\DeltaQ [w]')
set(gca,'XMinorTick','on','YMinorTick','on')
legend('\DeltaQ','\DeltaQ_{avg}=110 W')
% axis([0 7 0 300])


x=xlsread('NUS.xlsx','Sheet1','A3:E7');
time=x(:,1);
thi=x(:,2);
tho=x(:,3);
tci=x(:,4);
tco=x(:,5);
%ts=(x(:,5)+x(:,5))/2;
Del_T_Hot=thi-tho;
```

```
Del_T_Cold=tco-tci;
Cc=1.333360000000000e-05*996.6*4179;
Ch=0.0148*4183;
C_min=min(Cc,Ch);
DelT=thi-tci;
Q_max=C_min.*DelT;
Q_c=Cc.*Del_T_Cold;
Q_h=Ch.*Del_T_Hot;
e1=Q_c./Q_max*100;
e2=Q_h./Q_max*100;
e1_av=mean(e1);
e2_av=mean(e2);
ep=(e1_av+e2_av)./2;

LMTD=((thi-tci)-(tho-tco))./log((thi-tci)./(tho-tco));
A_s=0.047806897992273;
Q=(Q_h+Q_c)./2;
U=Q_c./(A_s*LMTD);
U_av=mean(U);

A_i=pi*.003*3;
h_i=mean(Q_h)/(A_i*mean(thi-tho));

A_o=pi*.005*3;
h_o=mean(Q_c)/(A_o*mean(tco-tci));

U_th=8.201195319681843e+02;
h_i_th=1.88e4;
h_o_th=991;
figure (1)
plot(time,thi,'*r-',time,tho,'*b-',time,tci,'*g-',time,tco,'*k-');
title('\DeltaT \color{red}(V=1 L/min)');
xlabel('Time [min]')
ylabel('T [C]')
legend('T_h_i','T_h_o','T_c_i','T_c_o')
% axis([0 14 0 30])
set(gca,'XMinorTick','on','YMinorTick','on')

figure (2)
plot(time,e1,'-r',time,e2,'-b',2.5,e1_av,'k*',2.5,e2_av,'g*')
xlabel('Time [min]')
ylabel('\epsilon','fontsize',24)
axis([0 7 0 100])
legend({'\epsilon=Q_c/Q_{max}','\epsilon=Q_h/Q_{max}','\epsilon_{av,}_{
Cold}','\epsilon_{av,}_{Hot}'},'fontsize',14,'location','best')
set(gca,'XMinorTick','on','YMinorTick','on')

figure (3)
c = categorical({'U_{Th}','U_{exp}'});
y = [U_th,U_av];
bar(c,y)
ylabel('Heat Transfer Co-efficient [W/m^2K]')


x=xlsread('US.xlsx','Sheet1','A3:E7');
time=x(:,1);
```

```
thi=x(:,2);
tho=x(:,3);
tci=x(:,4);
tco=x(:,5);
Del_T_Hot=thi-tho;
Del_T_Cold=tco-tci;
Cc=1.333600000000000e-05*996.6*4179;
Ch=0.0148*4183;
C_min=min(Cc,Ch);
DelT=thi-tci;
Q_max=C_min.*DelT;
Q_c=Cc.*Del_T_Cold;
Q_c1=mean(Q_c);
Q_h=Ch.*Del_T_Hot;
Q_h1=mean(Q_h);
LMTD=((thi-tci)-(tho-tco))./log((thi-tci)./(tho-tco));
A_s=0.047806897992273;
U=Q_c./(A_s*LMTD);
U_av=mean(U);
e1=Q_c./Q_max*100;
e2=Q_h./Q_max*100;
e1_av=mean(e1);
e2_av=mean(e2);

figure (1)
plot(time,thi,'-r*',time,tho,'-b*',time,tci,'-g*',time,tco,'-k*');
title('\DeltaT \color{red}(Q_c=0.8 L/min)');
xlabel('Time [min]')
ylabel('T [C]')
legend('T_h_i','T_h_o','T_c_i','T_c_o')
axis([0 7 20 40])
set(gca,'XMinorTick','on','YMinorTick','on')

figure (2)
plot(time,e1,'-r*',time,e2,'-b*',4,e1_av,'k*',4,e2_av,'g*')
xlabel('Time [min]')
ylabel('\epsilon','fontsize',24)
legend({'\epsilon=Q_c/Q_{max}','\epsilon=Q_h/Q_{max}','\epsilon_{av,}_{
Cold}','\epsilon_{av,}_{Hot}'},'fontsize',14,'location','best')
set(gca,'XMinorTick','on','YMinorTick','on')


%% NUS Case
x=xlsread('NUS.xlsx','Sheet1','A3:E7');
thi=x(:,2);
tho=x(:,3);
tci=x(:,4);
tco=x(:,5);
t=x(:,1);
%% Dimensions
L=3;
d_o=.005;
%% Flow Conditions
V=.8*1.6667e-5;      % Volume Flow rate
%% Properties
rho=996.6;
C_p=4179.2;        % Specific Heat
```

```
%% Ucertainties
U_v=1.05/100;
U_T=2/100;
U_d=.025e-3;
U_L=U_d;
%% Calculations
% Mass Flow Uncertainty
U_m=sqrt((rho)^2*(V*U_v)^2);
P_m=U_m/(rho*V)*100;
% Surface Area Uncertainty
U_As=sqrt((pi*L)^2*(U_d)^2+(pi*d_o)^2*(U_L)^2);
A_s=(pi*L*d_o);
P_As=U_As/A_s*100;
% Heat Transfer Uncertainty
U_Q=sqrt(((rho*V*C_p)^2*(U_T.*tco).^2)+((rho*V*C_p)^2*(U_T.*tci).^2)
...
                    +((C_p.*(tco-tci)).^2*(U_m)^2));
Q=(rho.*V.*C_p.*(tco-tci));
P_Q=U_Q./Q*100;
% LMTD uncertainty
U_LMTD=2/100;
LMTD=((thi-tci)-(tho-tco))./log((thi-tci)./(tho-tco));
% U Uncertainty
U_U=sqrt((1/(A_s.*LMTD)).^2*(U_Q).^2+(Q./(A_s^2.*LMTD)).^2*U_As.^2 ...
    +(Q./(A_s.*LMTD.^2)).^2.*(U_LMTD.*LMTD).^2);
U=Q./(A_s.*LMTD);
P_U=U_U./U*100;
P_Uav=mean(P_U);
% Q_max Uncertainty
C_min=61.9084;
Q_max=C_min.*(thi-tci);
U_Qmax=U_Q;
% Effectiveness Uncertainty
U_ep=sqrt((1./Q_max).^2.*(U_Q).^2+(Q./Q_max.^2).^2.*(U_Qmax).^2);
ep=Q./Q_max;
ep_av=mean(ep);
P_ep=U_ep./ep*100;
P_epav=mean(P_ep);
%% Temp NUS
% figure (1)
% errorbar(t,thi,U_T*thi,'-*')
% hold on
% errorbar(t,tho,U_T*tho,'-*')
% hold on
% errorbar(t,tci,U_T*tci,'-g*')
% hold on
% errorbar(t,tco,U_T*tco,'-k*')
% hold off
% xlim([0 7])
% xlabel('Time [min]')
% ylabel('Temperature [^oC]')
%% US Case
% Temp US
x=xlsread('US.xlsx','Sheet1','A3:E7');
thi=x(:,2);
tho=x(:,3);
tci=x(:,4);
```

```
tco=x(:,5);
t=x(:,1);
% U for US
LMTD_US=((thi-tci)-(tho-tco))./log((thi-tci)./(tho-tco));
Q_US=rho*V*C_p.*(tco-tci);
U_US=Q_US./(A_s.*(LMTD_US));
U_US=mean(U_US);
% Graph
% figure(2)
% errorbar(t,thi,U_T*thi,'-*')
% hold on
% errorbar(t,tho,U_T*tho,'-*')
% hold on
% errorbar(t,tci,U_T*tci,'-g*')
% hold on
% errorbar(t,tco,U_T*tco,'-k*')
% hold off
% xlim([0 7])
% xlabel('Time [min]')
% ylabel('Temperature [^oC]')
% U
U_NUS=811;
U_th=8.502874737532851e+02;
U_US=870;
figure (3)
c1=categorical({'Theoretical'});
c2 = categorical({'Non-Ultrasound'});
c3=categorical({'Ultrasound'});
x=[1,2];
y = [U_th,U_NUS,U_US];
bar(c1,U_th,'FaceColor','[0.8500 0.3250 0.0980]')
hold on
bar(c2,U_NUS,'FaceColor','blue')
hold on
bar(c3,U_US,'FaceColor','[0.4660 0.6740 0.1880]')
hold on
errorbar(2,U_NUS,P_Uav*U_NUS/100,'CapSize',10,'color','red','linewidth'
,2)
hold on
errorbar(3,U_US,P_Uav*U_US/100,'CapSize',10,'color','red','linewidth',2
)
hold off
ylabel('Overall Heat Transfer Coefficient U [W/m^2K]')
set(gca,'YMinorTick','on','linewidth',1.5,'FontName', 'Gill Sans
MT',...
    'FontSize',13)
%
ep_th=46.378002369843710;
ep_US=46.26;
ep_NUS=44.7;
figure (4)
c1=categorical({'Theoretical'});
c2 = categorical({'Non-Ultrasound'});
c3=categorical({'Ultrasound'});
bar(c1,ep_th,'FaceColor','[0.8500 0.3250 0.0980]')
hold on
bar(c2,ep_NUS,'FaceColor','blue')
```

```
hold on
errorbar(2,ep_NUS,P_epav*ep_NUS/100,'CapSize',10,'color','red','linewid
th',2)
hold on
bar(c3,ep_US,'FaceColor','[0.4660 0.6740 0.1880]')
hold on
errorbar(3,ep_US,P_epav*ep_US/100,'CapSize',10,'color','red','linewidth
',2)
hold off
ylim([0 60])
ylabel('Effectiveness \epsilon [Percent]')
set(gca,'YMinorTick','on','linewidth',1.5,'FontName', 'Gill Sans
MT',...
    'FontSize',13)
```